ASIA-PACIFIC JOURNAL OF MOLECULAR BIOLOGY AND BIOTECHNOLOGY

AsPac J. Mol. Biol. Biotechnol. 2025
ISSN: 0128-7451, eISSN: 2672-7277
Vol. 33 (1): 45-58
https://doi.org/10.35118/apjmbb.2025.033.1.06

RESEARCH ARTICLE

Structural and proteomic insights into the antibiofilm efficacy of DMSO on *Corynebacterium pseudotuberculosis*

Anati Abd Rashid Syaida[a], Mohd Izwan Mohammad Yusof[a], Faez Firdaus Abdullah Jesse[b], Nazia Abdul Majid[c], Mohd Fakharul Zaman Raja Yahya[a,d*]

[a]Faculty of Applied Sciences, Universiti Teknologi MARA Shah Alam, 40450 Shah Alam, Selangor, Malaysia
[b]Faculty of Veterinary Medicine, Universiti Putra Malaysia, 43400 UPM Serdang, Selangor, Malaysia
[c]Institute of Biological Sciences, Faculty of Science, Universiti Malaya, 50603 Kuala Lumpur, Malaysia
[d]Integrative Pharmacogenomics Institute (iPROMISE), 42300 Bandar Puncak Alam, Selangor, Malaysia
*Correspondence email: fakharulzaman@uitm.edu.my

Abstract

Corynebacterium pseudotuberculosis is an intracellular pathogen particularly responsible for causing caseous lymphadenitis in sheep and goats, resulting in substantial economic losses. Dimethyl sulfoxide (DMSO) has been shown to inhibit the formation of *C. pseudotuberculosis* biofilm. However, the molecular mechanisms underlying the antibiofilm efficacy of DMSO against *C. pseudotuberculosis* biofilm remain poorly understood. The present study was conducted to evaluate the inhibitory effects of DMSO on *C. pseudotuberculosis* biofilm and to determine the structural and proteomic changes in the biofilm following DMSO treatment. Pellicle assays, biomass assays, viability assays, FTIR spectroscopy, and FESEM were used to assess biofilm formation, biomass, viability, biochemical composition, and morphology of *C. pseudotuberculosis*, respectively. Additionally, one-dimensional SDS-PAGE in combination with tandem mass spectrometry and bioinformatics were performed to identify proteins expressed in *C. pseudotuberculosis* biofilm following treatment with 50% (v/v) DMSO. Results showed that DMSO treatment significantly inhibited the pellicle formation, biomass, and viability of *C. pseudotuberculosis* biofilm. Biochemical and morphological changes in *C. pseudotuberculosis* were observed following treatment with 50% (v/v) DMSO. 1D SDS-PAGE revealed differential protein expression in the range between 33.7 kDa and 150 kDa following treatment with 50% (v/v) DMSO. A total of 387 proteins were differentially expressed between the control and 50% (v/v) DMSO-treated biofilm. Analysis of the protein-protein interaction network of proteins with differential expression revealed that 50% (v/v) DMSO had an impact on 10 biological processes and 18 hub proteins. It is postulated that DMSO may inhibit *C. pseudotuberculosis* biofilm by modulating multiple biological pathways.

Keywords: biofilm, *Corynebacterium pseudotuberculosis*, dimethyl sulfoxide, protein expression, subtractive proteomics

INTRODUCTION

The bacterium *Corynebacterium pseudotuberculosis* is a Gram-positive, pleomorphic, and facultative intracellular pathogen that is classified under the order Actinomycetales. It is a stationary, β-hemolytic bacteria and a causative agent of livestock-related disorders (Domenis et al., 2018; Araújo et al., 2019). It can infect a wide range of animals but most commonly affects horses, camelids, cattle, and buffaloes (Dorella et al., 2006; Gomide et al., 2018; Tavares et al., 2024). As a prominent animal pathogen, *C. pseudotuberculosis* frequently causes a disease known as caseous lymphadenitis (CLA), primarily in sheep and goats, leading to significant economic losses. This infection results in decreased milk and wool production, weight loss, carcass condemnation, and potentially death (Dorella et al., 2006; Eberle et al., 2018; Domenis et al., 2018; El Damaty et al., 2023). Additionally, *C. pseudotuberculosis* can cause ulcerative lymphangitis, mastitis, and ulcerative dermatitis, all of which result in severe losses for the agricultural sector. Thus, *C. pseudotuberculosis* is a bacterium of veterinary

Received: 28 August 2024
Accepted: 23 February 2025
Published: 31 March 2025
Published by: Malaysian Society for Molecular Biology and Biotechnology (MSMBB)

significance (Dorella et al., 2006; Gomide et al., 2018). Our previous work characterized the structure and chemical composition of *C. pseudotuberculosis* biofilm (Yaacob et al., 2021). This biofilm formation enables *C. pseudotuberculosis* to persist on various surfaces, including veterinary equipment and environmental substrates, serving as reservoirs for infection. The EPS matrix impedes the penetration of antibiotics and shields the bacteria from the host's immune responses, leading to chronic and refractory infections. Within the host, *C. pseudotuberculosis* biofilm contributes to the development of encapsulated granulomas in lymph nodes and organs, characteristic of CLA (Idris & Arifah 2023). Consequently, the biofilm-forming capability of *C. pseudotuberculosis* is a critical factor in its infection success, contributing to persistent infections and significant economic losses in the livestock industry.

Dimethyl sulfoxide (DMSO) has been extensively studied for its potential applications in biofilm research (Lim et al., 2012; Yahya et al., 2017; Yaacob et al., 2021). Summer et al. (2022) showed that within specific ranges, DMSO can inhibit biofilm formation in various bacterial species, including clinically important species such as *Pseudomonas aeruginosa*. Schwarzer et al. (2021) demonstrated that the viable cells of *P. aeruginosa* and *Staphylococcus aureus* were completely eradicated upon exposure to a topical desiccating wound agent containing DMSO. The biofilm and planktonic fractions of *E. coli*, *P. aeruginosa*, and *Salmonella typhimurium* were also inhibited by 32% (v/v) DMSO (Yahya et al., 2018). To date, the molecular mechanism underlying the antibiofilm efficacy of DMSO against *C. pseudotuberculosis* biofilm is still poorly understood. Thus, the present study was conducted to assess the inhibitory effects of DMSO on *C. pseudotuberculosis* biofilm and to determine the structural and proteomic changes in the biofilm following DMSO treatment.

MATERIALS AND METHODS

Test compound

Solutions of dimethyl sulfoxide (Merck, Germany) were prepared within the volume range from 1.56% (v/v) to 50% (v/v).

Test microorganism

An isolated clinical strain of *C. pseudotuberculosis* was obtained from the Department of Veterinary Pathology and Microbiology at the Faculty of Veterinary Medicine, Universiti Putra Malaysia (UPM). The isolate was cultivated in bacterial Nutrient broth and kept at 37°C. Purity of the inoculum was routinely evaluated by Gram staining, examination of colony shape, and biochemical assays. The bacterial inoculum was calibrated to an optical density (OD) of 0.7 at 600 nm (1.2×10^9 CFU/mL) for all subsequent biological evaluations.

Pellicle assay

The pellicle test for *C. pseudotuberculosis* was conducted using the protocol described by Yaacob et al. (2021). Test tubes containing 4 mL of overnight *C. pseudotuberculosis* culture and 1 mL of DMSO solution were cultured in sterile conditions for a duration of 24 h. Following incubation at 37°C, the nutritional medium was disposed of. Following two rinses with sterile distilled water, the pellicle fractions were subjected to heat fixation at 60°C for 30 min which were then stained with 0.5% (w/v) crystal violet for 10 min. An antibiofilm cocktail protected by intellectual property (IP) was used a positive control. The pellicle fractions were then rinsed gently with sterile distilled water. The visual inspection of pellicle development was recorded.

Biomass assay

The biomass of *C. pseudotuberculosis* biofilm was evaluated using the crystal violet assay in a 96-well microplate according to Yahya et al. (2017). A total of 200 µL of overnight inoculum and 50 µL of DMSO solution were added to each well of the microplate. Additionally, a comparable amount of newly prepared broth and an antibiofilm mixture protected by intellectual property (IP) were used as negative and positive controls, respectively. Upon a 24 h incubation at 37°C, the medium containing the planktonic portion of *C. pseudotuberculosis* was removed, and the biofilm portions were carefully washed twice with sterile distilled water. The biofilm fractions were then subjected to an approximately 30 min heat fixation process using a Bunsen burner. The biofilm fractions were treated with a 0.5% (w/v) concentration of crystal violet for 5 min at ambient temperature and then thoroughly rinsed with sterile distilled water. The biofilm fractions underwent dissolution in 100% ethanol and were promptly quantified at a wavelength of 600 nm using a microplate reader manufactured by ThermoFisher Scientific, USA. Calculation of the % inhibition of biofilm biomass was performed using the mean absorbance values and the following equation:

$$\text{Percentage (\%) Inhibition} = \frac{(OD_{\text{negative control}} - OD_{\text{experimental}})}{OD_{\text{negative control}}} \quad (1)$$

Viability assay

The viability of *C. pseudotuberculosis* biofilm with and without dimethyl sulfoxide (DMSO) was evaluated using the resazurin assay in a 96-well microplate (Yaacob et al., 2021). A 0.02% (w/v) stock solution of resazurin was prepared and kept at 4°C in the absence of light. An overnight inoculum of 200 µL and 50 µL of DMSO solutions were introduced into the wells of the microplate. Positive controls were established by adding an equivalent amount of fresh broth and a proprietary antibiofilm mixture protected by intellectual property (IP). After an overnight incubation at 37°C, the medium was disposed of, and the microplate was washed twice with distilled water and then subjected to heat fixation at 60°C for 30 min. The biofilm fractions were dissolved in 220 µL of PBS buffer, and 30 µL of a 0.02% (w/v) solution of resazurin were introduced into the microwells. Following a minimum incubation period of 3 h at 37°C, the microplate was examined at 570 nm using a microplate reader manufactured by ThermoFisher Scientific in the United States. . Calculation of the % inhibition of biofilm biomass was performed using the mean absorbance values and the following equation:

$$\text{Percentage (\%) Inhibition} = \frac{(OD_{\text{negative control}} - OD_{\text{experimental}})}{OD_{\text{negative control}}} \quad (2)$$

Biofilm imaging

A study of the structure of *C. pseudotuberculosis* biofilm was conducted using a field emission scanning electron microscope (FESEM) from Hitachi, Japan, following the methodology described by Yaacob et al. (2021). Sterile glass coverslips were placed in each well of a 6-well microplate with the surface of interest orientated upwards. Then, a total of 4 mL of overnight inoculum and 1 mL of 50% (v/v) DMSO were added to each well. Overnight incubation of the microplate was carried out at 37°C. The glass coverslips were then removed from the microplate and were washed twice with phosphate-buffered saline. The biofilm on the coverslip was then preserved in a 4% (v/v) formaldehyde solution at 4°C for 3 h. Upon rinsing with sterile distilled water tree times, the coverslips were dehydrated in ethanol solutions of 25% (v/v), 50% (v/v), 75% (v/v), and 100% (v/v) for 10 min per concentration. The coverslips were led to air dry overnight and were then examined using a Field Emission Scanning Electron Microscope (FESEM) at 10,000× magnification.

Fourier transform infrared spectroscopy

Analysis of the biochemical composition of *C. pseudotuberculosis* biofilm was performed using a ThermoScientific NICOLET 6700 ATR-FTIR spectrometer (Thermo Fisher Scientific Inc., USA) (Yahya et al., 2017). A total of 4 mL of overnight inoculum and 1 mL of 50% (v/v) DMSO were added to each well of a 6-well microplate. Following a 24 h incubation at 37°C, the nutritional medium was then disposed of. The biofilm fractions underwent two separate rinses with sterile distilled water, followed by overnight heat-drying at 60°C, and finally scraping off from the microplate. The completely desiccated biofilm portions were brought into direct contact with a diamond crystal and subjected to scanning throughout the 4,000 to 600 cm^{-1} range, with a resolution of 2 cm^{-1}. The IR spectra underwent automated baseline correction and normalisation to get a spectrum of the biofilm.

Protein extraction and determination

Extraction of biofilm proteins followed the optimized protocol by Yahya et al. (2017). *C. pseudotuberculosis* was grown as described above in the absence and presence of 50% (v/v) DMSO and incubated for 24 h at 37°C. The nutrient medium was then discarded, and the wells were rinsed twice with distilled water. A total of 1.5 mL of saline buffer was added to the wells to resuspend the biofilm fraction. The biofilm fraction was then transferred to a microcentrifuge tube and pelleted at 10,000 rpm for 10 min. The resulting pellet was incubated in 1,000 µL of lysis buffer consisting of 25 mM Tris, 150 mM NaCl, 0.5% (w/v) SDS, and 10 µL of 1 mM PMSF at 95°C for 15 min. Following incubation, the whole-cell fraction was pelleted again at 10,000 rpm for 10 min. Protein amount was determined using standard Bradford assay.

One dimensional SDS-PAGE

The separation of biofilm proteins was carried out following the method described by Yahya et al. (2017). Protein samples were dissolved in 10 µL of Laemmli sample buffer and 2 µL of β-mercaptoethanol (BME), which were then subjected to a temperature of 95 degrees Celsius for a duration of 5 min. Using the Mini-PROTEAN Tetra Cell, the protein samples were placed into individual wells of a 12% (w/v) Mini-PROTEAN TGX precast protein gel. The experiment was repeated three times using a reaction mixture of 192 mM glycine, 25 mM Tris, and 0.1% (w/v) SDS. The electrophoresis was set at 100 V for 90 min until the blue dye front reached the bottom of the polyacrylamide gel. The protein samples were analysed using the Precision Plus

Protein Dual Colour Standard with a mass range of 10-250 kDa. The gel was stained using a Coomassie Brilliant Blue R-250 staining solution kit following the recommended guidelines provided by the manufacturer. Prior to staining for about 1 h, the gel was rinsed with deionised water. Following staining, the gel was rinsed two times on an orbital shaker. The pigment from the gel was removed by immersing it in a destaining solution and gently agitating it for 1 h at 60 rpm. The gel was examined using the Gel Doc EZ Imager, followed by densitometric analysis using ImageJ software. Once manual excising was completed, all protein bands underwent trypsin digestion and protein identification using LC-MS/MS.

Statistical analysis

The densitometric analysis data was reported as the mean ± standard deviation for a sample size of n = 3. The statistical significance of the differences between the control and test groups was evaluated using an independent T-test, with a p-value less than 0.05 being significant.

Trypsin digestion

Protein bands were destained with a 25 mM solution of ammonium bicarbonate in a 50:50 blend of acetonitrile and hydrodistilled water for a duration of 45 min. The protein bands were then kept at -20°C after being vacuum-dried. Approximately 10 µL of solution (12.5 µg of trypsin in 25 mM ammonium bicarbonate) was applied to each gel slice and left for incubation at 37°C overnight. Following digestion, the peptides were subjected to a 20-min incubation with 10 µL of acetonitrile containing 1% (w/v) trifluoroacetic acid. Furthermore, the peptides were desalted using a C18 ZipTip (Millipore) and dried using a Speed-Vac concentrator at an ambient temperature. The concentration of eluted peptides was determined using a NanoDrop spectrophotometer to establish the conditions for tandem mass spectrometry.

High-performance liquid chromatography-tandem mass spectrometry

HPLC-MS/MS was used to identify proteins expressed in the biofilm of *C. pseudotuberculosis*. The nano high-performance liquid chromatography (HPLC) system, in conjunction with the TripleTOF 5600 Plus Mass Spectrometer (AB SCIEX, USA), was used to analyse the tryptic peptides. The TripleTOF 5600 mass spectrometer was configured according to (Yahya et al., 2017) whilst proteins of interest were identified by subjecting QTOF mass spectra to analysis using Matrix Science and the SwissProt database. To achieve high-confidence protein identification, proteins that were identified by two or more peptides were chosen.

Bioinformatics

Proteins which were expressed differently in the biofilm of *C. pseudotuberculosis* after treatment with 50% (v/v) DMSO were classified using the UniProt/TrEMBL database. Subcellular localisation prediction was performed using the CELLO2GO website. An analysis of the protein-protein interaction network of the *C. pseudotuberculosis* proteins was performed using the STRING database version 11.0. The confidence threshold for the study of protein interaction networks was established at a conservative level of 0.7. The analysis was conducted using neighbourhood data, fusion-fission events, occurrence frequencies, co-expression patterns, text mining techniques, and data obtained from public databases of physical encounters. Functional gene ontology (GO) enrichment studies were also conducted to identify significant ($p < 0.05$) biological processes linked to the protein network.

RESULTS

Pellicle formation

C. pseudotuberculosis formed the pellicle at air-liquid interface after 24 h at 37°C (Figure 1). It was found that the intensity of the pellicle at the air-liquid interface apparently decreased as the concentration of DMSO increased from 1.56% (v/v) to 50% (v/v).

DMSO inhibits the biomass of C. pseudo-tuberculosis biofilm

The percentage of biomass inhibition ranged from 62.7% to 84.6% (Figure 2). DMSO at 50% (v/v) exhibited the greatest biofilm percentage suppression, followed by DMSO at 25% (v/v) and DMSO at 12.5% (v/v). Significant inhibition of *C. pseudotuberculosis* biofilm was observed at all test concentrations ($p < 0.05$).

DMSO inhibits the viability of C. pseudo-tuberculosis biofilm

The viability of C. *pseudotuberculosis* biofilm was significantly inhibited ($p < 0.05$) by 50% (v/v) DMSO (Figure 3). Inhibiting the viability leads to prevention of *C. pseudotuberculosis*'s growth and disruption of biofilm integrity.

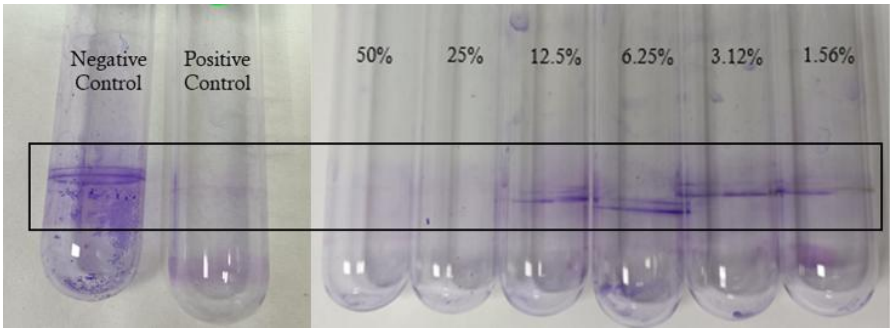

Figure 1. The pellicle formation at air-liquid interface by *C. pseudotuberculosis* biofilm

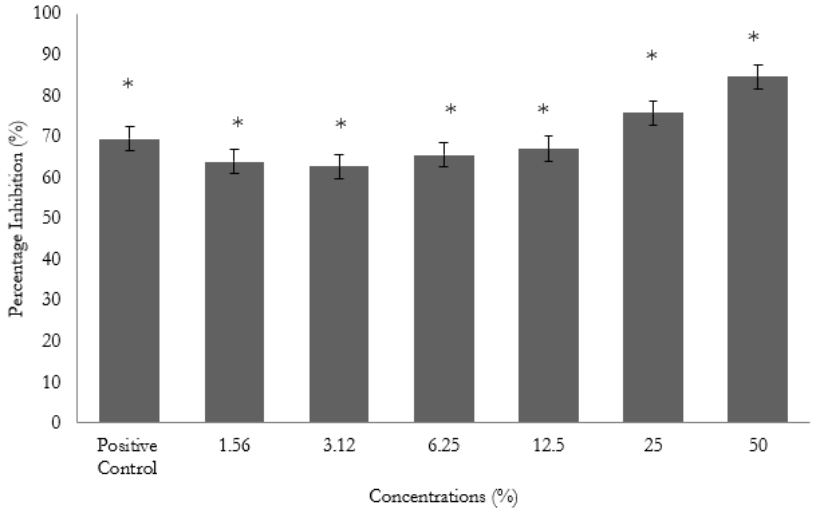

Figure 2. Percentage of *C. pseudotuberculosis* biofilm biomass following treatment with different concentrations of DMSO. Positive control: overnight inoculum added with IP-protected antibiofilm cocktail. Each bar represents mean ± standard deviation. Significant differences ($p < 0.05$) when compared with control group are shown by *.

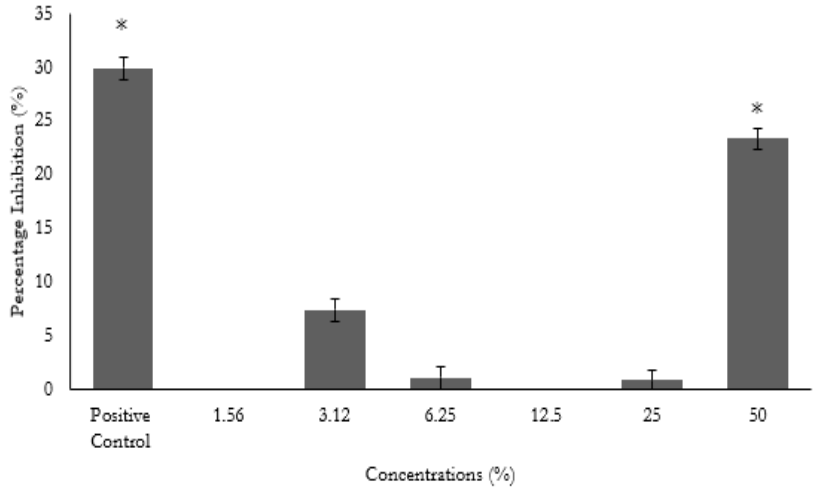

Figure 3. The viability of *C. pseudotuberculosis* biofilm following treatment with different concentrations of DMSO. Positive control: Intellectual property (IP) – protected antibiofilm cocktail. Each bar represents mean ± standard deviation. Significant differences ($p<0.05$) when compared with control group are shown by *.

DMSO modifies the morphology of C. pseudotuberculosis biofilm

At a magnification of 10,000×, the well-defined rod-shaped *C. pseudotuberculosis* cells were surrounded by heterogenous extracellular matrix throughout the biofilm structure (Figure 4). This typical biofilm morphology suggests strong cell-to-cell adhesion and biofilm integrity. Treatment with 50% (v/v) DMSO resulted in less distinct cell boundaries and some cells appeared to deform and lyse. This disrupted morphology indicates that the treatment has effectively interfered with the biofilm's structural integrity, possibly leading to biofilm dispersal or cell death.

DMSO alters biochemical composition of C. pseudotuberculosis biofilm

Treatment with 50% (v/v) DMSO altered the FTIR spectra in the range between 3,500 cm^{-1} and 800 cm^{-1} (Figure 5). Notable changes were observed in the spectral peak shapes at 1,040 cm^{-1}, 1,380 cm^{-1}, 1,410 cm^{-1}, and 3,272 cm^{-1} in the *C. pseudotuberculosis* biofilm when treated with 50% (v/v) DMSO. Additionally, the spectral peak at 1,652 cm^{-1} shifted to 1,639 cm^{-1}, while the spectral peak at 2,930 cm^{-1} completely disappeared. These spectral peaks correspond to functional groups associated with proteins, lipids, nucleic acids, and polysaccharides, which constitute the extracellular matrix of the *C. pseudotuberculosis* biofilm (Table 1).

Proteome profile

The protein profiling of *C. pseudotuberculosis* control biofilm (left) and 50% (v/v) DMSO-treated biofilm (right) are shown in Figure 6. Both control biofilm and 50% (v/v) DMSO-treated biofilm showed nine proteins ranging between 3.7 kDa and 150 kDa. The intensity of *C. pseudotuberculosis* two proteins bands (33.7 kDa and 41.9kDa) in control biofilm were significantly ($p < 0.05$) higher in control biofilm compared to 50% (v/v) DMSO-treated biofilm (Figure 7). This result provides a preliminary insight that certain metabolic pathways within *C. pseudotuberculosis* biofilm are being downregulated in response to 50% (v/v) DMSO.

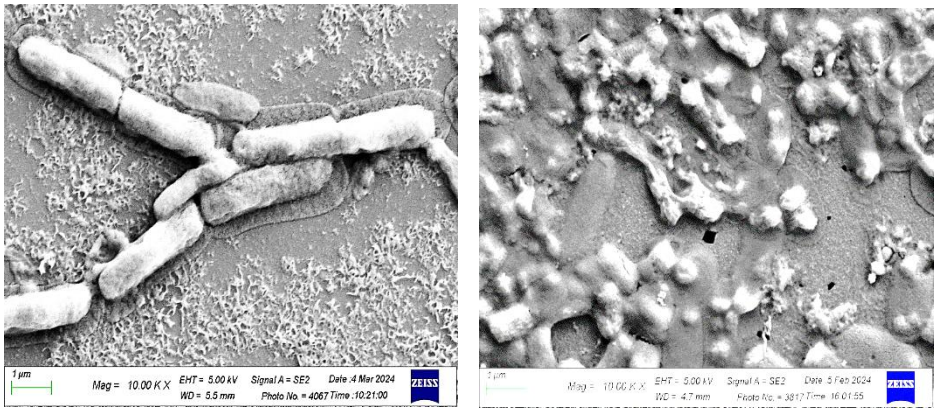

Figure 4. The normal morphology of *C. pseudotuberculosis* biofilm at 10,000X magnification (Left). The morphology of *C. pseudotuberculosis* treated with 50% (v/v) DMSO (Right).

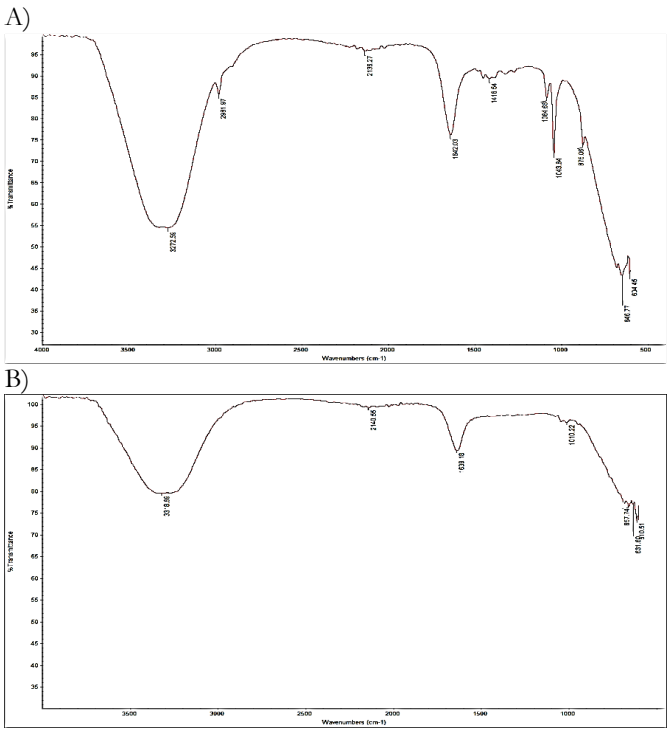

Figure 5. (A) FTIR spectrum of control *C. pseudotuberculosis* biofilm, (B) FTIR spectrum of *C. pseudotuberculosis* biofilm treated with 50% (v/v) DMSO.

Table 1. FTIR assignment of functional groups contained in *C. pseudotuberculosis* biofilm.

Wavenumber (cm^{-1})	IR Assignment	Classification	References
1040	C-O & C-O-C stretching (carbohydrates)	polysaccharides, nucleic acids	Mihoubi et al. (2017) Yahya et al. (2017) Dzurendova et al. (2020)
1380	(C-N stretching vibration/N-H bending vibration) Amide III	proteins	Kamaruzzaman et al. (2022)
1410	C=O symmetric stretching of COO- group	lipids, proteins	DeQueiroz & Day (2007)
1652	C-O stretching (amide I)	proteins	Chen et al. (2015) Yahya et al. (2017) Mihoubi et al. (2017) Maddela (2018) Dzurendova et al. (2020)
2930	C-H stretching	lipids	Sheng et al. (2006)
3272	O-H bond (hydroxyl group)	polysaccharides, nucleic acids, proteins, lipids	The present study

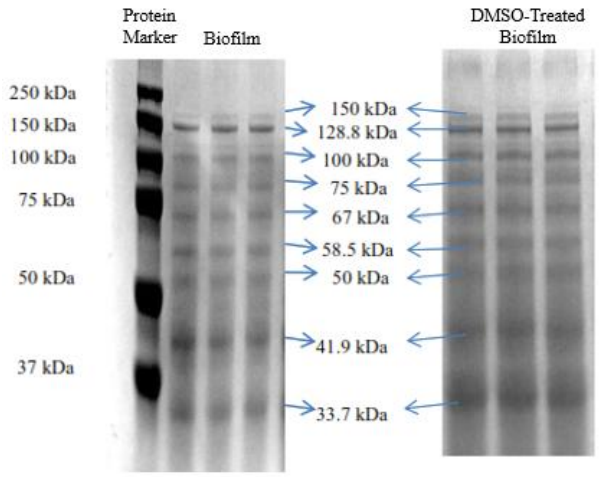

Figure 6. Protein profile of control *C. pseudotuberculosis* biofilm (Left). Protein profile of 50% (v/v) DMSO-treated *C. pseudotuberculosis* biofilm (Right).

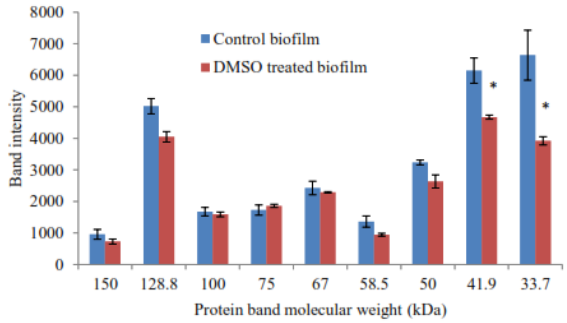

Figure 7. Intensity of *C. pseudotuberculosis* proteins bands in control biofilm and 50% (v/v) DMSO-treated biofilm. Each bar represents mean ± standard deviation. Significant differences ($p < 0.05$) when compared with control group are shown by *.

Distribution of identified C. pseudotuberculosis proteins

The Venn diagram shows identified *C. pseudotuberculosis* proteins in control biofilm and 50% (v/v) DMSO-treated biofilm (Figure 8). A total of 494 and 289 proteins were successfully identified in control biofilm and 50% (v/v) DMSO-treated biofilm, respectively. Of these, 296 proteins (50.6%) were exclusively expressed in the control biofilm, while 91 proteins (15.6%) were exclusively expressed in the 50% (v/v) DMSO-treated biofilm. Meanwhile, 198 proteins (33.8%) were found to overlap in both control and 50% (v/v) DMSO-treated biofilms.

Treatment with 50% (v/v) DMSO triggers differential expression of C. pseudotuberculosis biofilm proteins

A total of 387 differentially expressed *C. pseudotuberculosis* proteins were successfully identified using a subtractive proteome approach, considering only proteins expressed in either the control or treated biofilm (Supplementary file 1). Most of these proteins were associated with metabolic pathways (Figure 9) and located in the cytoplasm (Figure 10). Differential protein expression is associated with the impaired ability of *C. pseudotuberculosis* to form pellicle and biofilm.

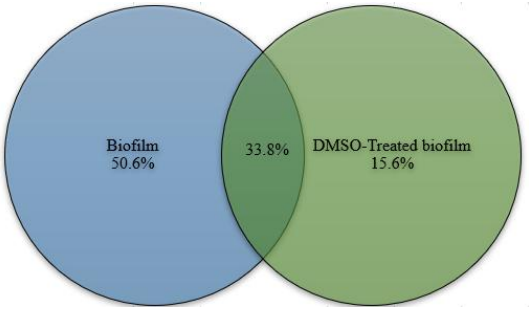

Figure 8. Venn diagram for identified *C. pseudotuberculosis* proteins in control and 50% (v/v) DMSO-treated biofilms.

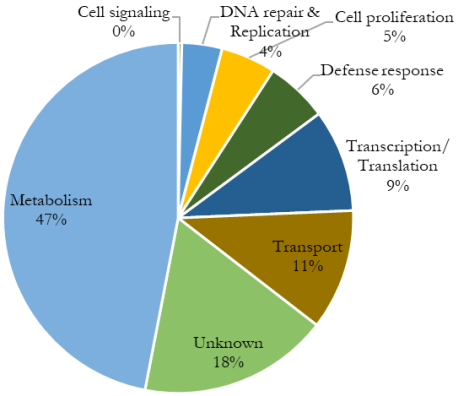

Figure 9. Classification of differentially expressed proteins in *C. pseudotuberculosis* biofilm following treatment with 50% (v/v) DMSO.

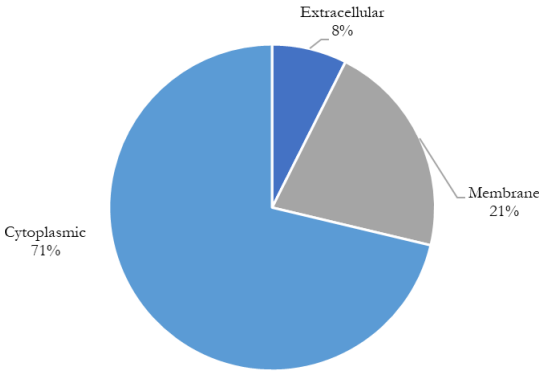

Figure 10. Subcellular localization of differentially expressed proteins in *C. pseudotuberculosis* biofilm following treatment with 50% (v/v) DMSO.

Protein-protein interaction networks

STRING analysis revealed a total of 920 functional interactions among the differentially expressed *C. pseudotuberculosis* proteins (Figure 11). Significant ($p < 0.05$) molecular functions and biological processes in the protein-protein interaction networks affected by 50% (v/v) DMSO are shown in Table 2 and Table 3, respectively.

Hub C. pseudotuberculosis biofilm proteins affected by 50% (v/v) DMSO

Based on the networks, a total of 18 hub proteins (nodes with more than 10 functional interactions) in *C. pseudotuberculosis* biofilm were found to be affected by 50% (v/v) DMSO (Table 4). Inhibiting them can disrupt key metabolic networks, potentially impairing *C. pseudotuberculosis*'s ability to survive or replicate.

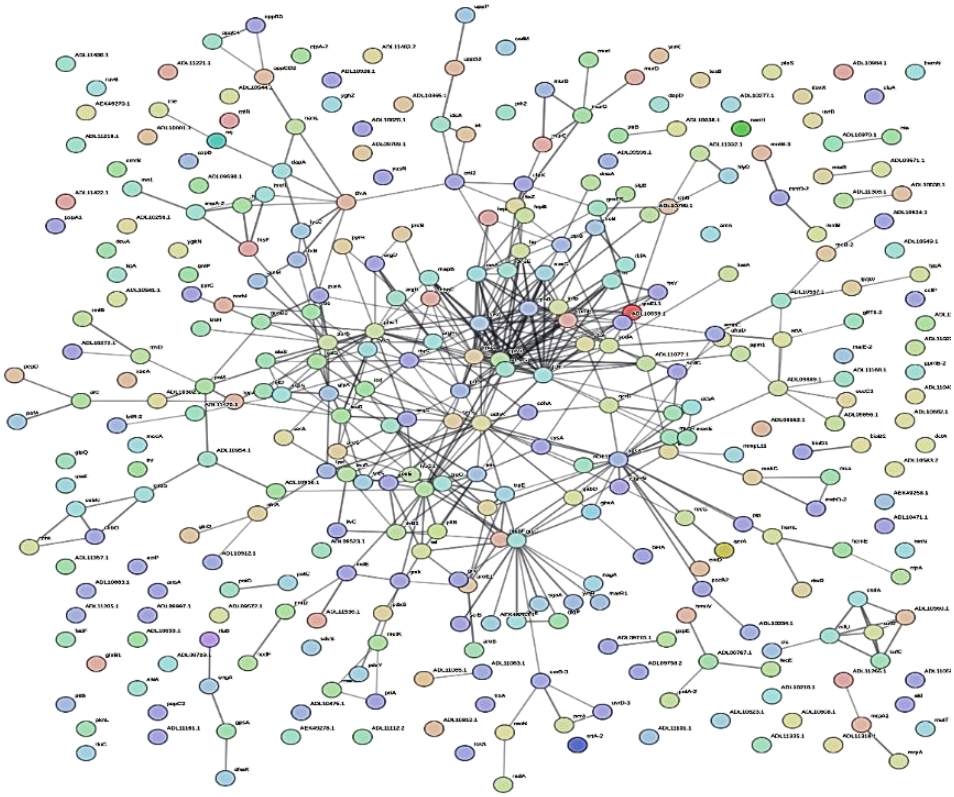

Figure 11. Functional interactions of differentially expressed *C. pseudotuberculosis* biofilm proteins.

Table 2. Enrichment analysis of the molecular function using gene ontology.

GO Molecular function	Observed protein count	*p*-value
Catalytic activity	234	1.28E-08
Small molecule binding	105	5.27E-06
Nucleotide binding	94	1.36E-05
Ion binding	133	1.36E-05
Ribonucleotide binding	80	0.00019
Purine ribonucleoside triphosphate binding	79	0.00019
Carbohydrate derivative binding	81	0.00019
ATP binding	70	0.0011
Organic cyclic compound binding	130	0.0035
Heterocyclic compound binding	130	0.0035
Nucleoside-triphosphatase activity	20	0.0066
Pyrophosphatase activity	21	0.0196
aminoacyl-tRNA ligase activity	12	0.0215
ATP hydrolysis activity	13	0.0231
Oxidoreductase activity	44	0.0365

Table 3. Enrichment analysis of the biological process using gene ontology.

GO Biological Process	Observed protein count	*p*-value
Cellular process	257	4.51E-07
Metabolic process	222	2.66E-05
Organic substance metabolic process	196	0.0024
Biosynthetic process	116	0.0066
Cellular amino acid metabolic process	42	0.0101
Nitrogen compound metabolic process	150	0.0268
Carboxylic acid metabolic process	57	0.0268
Cellular aromatic compound metabolic process	92	0.043
Organic cyclic compound metabolic process	95	0.043
Organonitrogen compound biosynthetic process	81	0.043

Table 4. List of hub proteins based on protein-protein interaction networks.

Node	Number of functional interactions	Protein Identity
purB	10	Adenylosuccinate lyase
infB	11	Translation initiation factor IF-2
soda	11	Manganese superoxide dismutase
leuS	12	Leucyl-tRNA synthetase
thrS	12	Threonyl-tRNA synthetase
rpsA	13	30S ribosomal protein S1
Pyk	14	Pyruvate kinase
rpmB	14	50S ribosomal protein L28
ptsG	18	Phosphotransferase system II component
odhA	19	2-oxoglutarate dehydrogenase E1 component
rplW	19	50S ribosomal protein L23
rplA	20	50S ribosomal protein L1
fusA	21	Elongation factor G
pheT	21	Phenylalanyl-tRNA synthetase beta chain
ppsA	21	Phthiocerol synthesis polyketide synthetase type I PpsA
rpoB	21	DNS-directed RNA polymerase subunit beta
rpsG	22	30S ribosomal protein S7
rplF	23	50S ribosomal protein L6

DISCUSSION

Combating pathogenic biofilms is critical due to their role in chronic infections and resistance to conventional treatments. Biofilms are structured microbial communities encased in an extracellular polymeric matrix, which protects bacteria from antibiotics and immune responses, making infections harder to treat. Addressing this challenge requires diverse and innovative approaches. Antibiotics remain a foundational strategy, but their efficacy is often limited against biofilm-embedded bacteria. Plant extracts, nanoparticles, and polymers, hold promise in medical and industrial applications by preventing bacterial adhesion and biofilm maturation (Yakup et al., 2024; Yahya et al. 2024). By integrating these strategies, biofilm-associated infections can be effectively addressed, reducing their impact on human health, animal health and industry.

In an aerobic environment, biofilms tend to form a pellicle at the air-liquid interface, which gives a cloudy appearance. In the present study, treatment with 50% (v/v) DMSO significantly ($p < 0.05$) inhibited pellicle formation at the air-liquid interface, as well as the biofilm biomass and viability of *C. pseudotuberculosis*. The obtained results align with the conclusions of Yaacob et al. (2021), who showed that DMSO effectively suppressed the development of *C. pseudotuberculosis* biofilm at all concentrations examined. When tested against three different strains of biofilm-forming bacteria (*Escherichia coli, Klebsiella pneumoniae, Pseudomonas aeruginosa*), Lončar et al. (2017) found that DMSO significantly decreased preformed biofilm biomass and viable colony-forming units compared to other antimicrobial agents such as ozone, hypochlorous agents, and antimicrobial peptide mimics.

The morphology of *C. pseudotuberculosis* was investigated in this work using FESEM. This selection was made because FESEM can overcome resolution limitations by utilising an electron beam, enabling high-magnification analyses of various biofilm components, cell-to-cell interactions, and extracellular matrix components (Habimana et al., 2009). In the present study, *C. pseudotuberculosis* was found to form a thin layer on the surface. However, the biofilm structure was completely disrupted when treated with 50% (v/v) DMSO. This result is consistent with the conclusions of Herasimenka et al. (2008), who suggested that DMSO causes the degradation of polymer chain aggregation in polysaccharides, resulting in the scattering of polymer chains and the creation of a permeable biofilm.

Fourier Transform Infrared (FTIR) spectroscopy is a method used to determine the chemical composition and structure of a sample by measuring its infrared spectrum. It has increasingly become an important tool for studying antibiofilm mechanisms (Kamaruzzaman et al., 2022; Johari et al., 2023; Hamdan et al., 2024). In the present study, significant changes were observed in the intensity and position of several FTIR spectral peaks of 50% (v/v) DMSO-treated biofilm compared to the control. The peaks corresponding to lipids, proteins, nucleic acids, and carbohydrates showing changes may indicate structural alterations or degradation due to the 50% (v/v) DMSO treatment. These spectral changes provide insight into the molecular mechanisms underlying the observed biofilm disruption upon 50% (v/v) DMSO treatment. DMSO has been reported to cause conformational changes in proteins and nucleic acids, as well as alter the fluidity of lipid membranes and disrupt polysaccharide chains (Batista et al., 2013; Xu et al., 2016).

The ESI–QTOF technique is an excellent analytical approach for determining the identity of proteins. This technology offers many benefits, including a rapid data capture rate, remarkable resolution, and exceptional mass accuracy. In the present study, the ESI-QTOF technique was used to identify differentially expressed *C. pseudotuberculosis* proteins between control and 50% (v/v) DMSO-treated biofilms. The identified *C. pseudotuberculosis* proteins, such as superoxide dismutase, pyruvate kinase, serine/threonine protein kinase, isocitrate dehydrogenase, ATP synthase subunit beta, and 30S ribosomal protein, have also been expressed in other microbial biofilms (Zawawi et al., 2020; Santi et al., 2024; Zulkiply et al., 2024).

ABC transporters are a diverse superfamily of proteins found in all domains of life, playing crucial roles in bacterial pathogenesis and virulence (Akhtar & Turner, 2022). These transporters utilize ATP hydrolysis to facilitate the import of essential molecules like metal ions, amino acids, and vitamins, as well as the export of virulence factors and toxic substances. The present study demonstrated inhibited expression of ABC transporter permease in *C. pseudotuberculosis* biofilm following treatment with 50% (v/v) DMSO. This finding is consistent with Yahya et al. (2017), who also reported inhibited expression of ABC transporter permease in *S. typhimurium* biofilm treated with 32% (v/v) DMSO.

Phosphoglycerate dehydrogenase plays an important role in bacterial metabolism, including gluconeogenesis, glycolysis, and phosphorylation. In the present study, the expression of phosphoglycerate dehydrogenase was suppressed in the 50% (v/v) DMSO-treated biofilm. Yahya et al. (2017) also showed that the expression of phosphoglycerate dehydrogenase in *Salmonella typhimurium* biofilm was inhibited by treatment with 32% (v/v) DMSO.

Biofilm communities exhibit complex metabolic dynamics and protein expression patterns during dormancy. Dormant biofilm cells are known to show reduced ribosome synthesis and altered purine, arginine, and proline metabolism (Carvalhais et al., 2015). In the present study, protein metabolism in *C. pseudotuberculosis* biofilm was inhibited by treatment with 50% (v/v) DMSO. Similarly, this metabolic pathway in *S. typhimurium* biofilm was inhibited by 32% (v/v) DMSO. The inhibition of protein metabolism in biofilms by small molecules has also been reported by Campbell et al. (2024). According to Krátk et al. (2023), the inhibition of protein metabolism could reduce biofilm viability.

Functional interactions were observed among differentially expressed *C. pseudotuberculosis* proteins in the protein-protein interaction networks. A total of 18 hub proteins were identified in these functional networks and were found to inhibited by 50% (v/v) DMSO. One of these is the 50S ribosomal protein L1 (rplA), which participates in the translation process. Hub proteins, which have numerous functional interactions within the networks, are increasingly recognized as potential drug targets (Isa et al., 2022; Nematiasgarabad et al., 2024). These hubs play crucial roles in network stability and function (Patil et al., 2010). Folador et al. (2016) found that rplA is a non-host homologous protein without any significant hits against at least one host. Non-host homologous proteins in *C. pseudotuberculosis* are potential targets for therapeutic and diagnostic purposes (Abd Rashid et al., 2022).

The study's findings on the inhibitory effects of dimethyl sulfoxide (DMSO) on *C. pseudotuberculosis* biofilms offer promising avenues for treating CLA caused by this pathogen. Biofilms protect bacteria from antibiotics and immune responses, complicating

treatment efforts. The study demonstrated that DMSO disrupts the biofilm's extracellular polymeric substance matrix and alters bacterial cell membranes, enhancing the efficacy of antimicrobial agents. Proteomic analyses revealed that DMSO affects expression of important proteins, such as ABC transporter and phosphoglycerate dehydrogenase, which are crucial for biofilm maintenance and virulence. By targeting these proteins, DMSO not only impairs biofilm integrity but also reduces the bacterium's ability to cause disease. These insights suggest that incorporating DMSO into treatment protocols could improve outcomes for infections associated with *C. pseudotuberculosis,* particularly in veterinary settings where CLA poses significant challenges. Previous studies reported low systemic toxicity *in vivo* and safe application of DMSO (up to 50% concentration) for oral and topical treatments (Zuurmond et al. 1996; Capriotti & Capriotti 2012). However, further *in vivo* studies are necessary to confirm antibiofilm efficacy of DMSO in clinical applications

CONCLUSION

The present study demonstrated the influence of DMSO on the pellicle, biomass, viability, morphology, and biochemical composition of *C. pseudotuberculosis* biofilm. Following treatment with 50% (v/v) DMSO, the proteome profile of *C. pseudotuberculosis* biofilm exhibited significant changes, with differentially expressed proteins indicating alterations in multiple biological pathways. The protein-protein interaction networks within the biofilm were also affected, suggesting disruption of biofilm formation by 50% (v/v) DMSO. These findings imply that 50% (v/v) DMSO modulates key biological processes, potentially inhibiting biofilm formation in *C. pseudotuberculosis*. Integrating DMSO into treatment strategies has the potential to enhance the management of *C. pseudotuberculosis* infections, particularly in veterinary contexts where CLA presents substantial challenges.

ACKNOWLEDGEMENT

The authors are highly grateful to the Faculty of Applied Sciences, Universiti Teknologi MARA Shah Alam and Faculty of Veterinary Medicine, Universiti Putra Malaysia, for providing research facility and test microorganism, respectively. This research was funded by Malaysia Ministry of Higher Education under a research grant, 600-IRMI/FRGS 5/3 (417/2019).

CONFLICT OF INTEREST

The authors have declared that no conflict of interest exists.

REFERENCES

Akhtar, A. A., & Turner, D. P. (2022). The role of bacterial ATP-binding cassette (ABC) transporters in pathogenesis and virulence: Therapeutic and vaccine potential. *Microbial Pathogenesis 171*, 105734. https://doi.org/10.1016/j.micpath.2022.105734

Abd Rashid, S. A., Yaacob, M. F., Raihanah, N., Anuar, T., Johari, N., Kamaruzaman, A. N. A., ... & Yahya, M. F. Z. R. (2022). A combination of in silico subtractive and reverse vaccinology approaches reveals potential vaccine targets in Corynebacterium pseudotuberculosis. *Journal of Sustainability Science and Management 17*(1), 99-109. http://doi.org/10.46754/jssm.2022.01.007

Araújo, L., Alves, J., Nogueira, W., Pereira, L. C., Gomide, A. C., Ramos, R., Azevedo, V., Silva, A., & Folador, A. (2019). Prediction of new vaccine targets in the core genome of *Corynebacterium pseudotuberculosis* through omits approaches and reverse vaccinology. *Gene 702*(12), 36-45. https://doi.org/10.1016/j.gene.2019.03.049

Batista, A. N., Batista Jr, J. M., Bolzani, V. S., Furlan, M., & Blanch, E. W. (2013). Selective DMSO-induced conformational changes in proteins from Raman optical activity. *Physical Chemistry Chemical Physics 15*(46), 20147-20152. https://doi.org/10.1039/C3CP53525H

Campbell, M. J., Beenken, K. E., Spencer, H. J., Jayana, B., Hester, H., Sahukhal, G. S., ... & Smeltzer, M. S. (2024). Comparative evaluation of small molecules reported to be inhibitors of Staphylococcus aureus biofilm formation. *Microbiology Spectrum 12(*1), e03147-23. https://doi.org/10.1128/spectrum.03147-23

Capriotti, K., Capriotti, J. A. (2012). Dimethyl sulfoxide: history, chemistry, and clinical utility in dermatology. *The Journal of Clinical and Aesthetic Dermatology 5*, 24–26.

Carvalhais, V., Cerca, N., Vilanova, M., & Vitorino, R. (2015). Proteomic profile of dormancy within Staphylococcus epidermidis biofilms using iTRAQ and label-free strategies. *Applied Microbiology and Biotechnology 99*, 2751-2762. https://doi.org/10.1007/s00253-015-6434-3

Chen, Y., Zou, C., Mastetalerz, M., Hu, S., Gasaway, C., & Tao, X. (2015). Applications of Micro-Fourier Transform Infrared spectroscopy (FTIR) in the geological sciences - A review. *International Journal of Molecular Sciences 16*(12), 30223-30250. https://doi.org/10.3390/ijms161226227

DeQueiroz, G. A., & Day, D. F. (2007). Antimicrobial activity and effectiveness of a combination of sodium hypochlorite and hydrogen peroxide in killing and removing *Pseudomonas aeruginosa* biofilms from surfaces. *Journal of Applied Microbiology 103*(4), 794-802. https://doi.org/10.1111/j.1365-2672.2007.03299.x

Domenis, L., Spedicato, R., Pepe, E., Orusa, R., & Robetto, S. (2018). Caseous lymphadenitis caused by *Corynebacterium pseudotuberculosis* in alpine chamois (*Rupicapra r. rupicapra*): A review of 98 cases. *Journal of Comparative Pathology 161*, 11-19. https://doi.org/10.1016/j.jcpa.2018.04.003

Dorella. F. A., Pacheco, L. G. C., Oliveira, S. C., Miyoshi, A., & Azevedo, V. (2006). *Corynebacterium pseudotuberculosis*: microbiology, biochemical properties, pathogenesis and molecular studies of virulence. *Veterinary Research 37* (2), 201-218. https://dx.doi.org/10.1051/vetres:2005056

Dzurendova, S., Zimmermann, B., Kohler, A., Tafintseva, V., Slany, O., Certik, M. & Shapaval, V. 2020. Microcultivation and FTIR spectroscopy-based screening revealed a nutrient-induced co-production of high-value metabolites in oleaginous *Mucoromycota* fungi. *PloS ONE 15*(2), e0245016. https://doi.org/10.1371/journal.pone.0234870

Eberle, R. J., Kauai, L. A., Moraes, F. R. D., Olivier, D., Amaral, M. S. D., Tasic, L., Arni, R. K. & Coronado, M. A. (2018). Inhibition of this redo in A1 from *Corynebacterium pseudotuberculosis* by polyanions and flavonoids. *International Journal of Biological Macromolecules 117* (2), 1066-1073. https://doi.org/10.1016/j.ijbiomac.2018.06.022

El Damaty, H. M., El-Demerdash, A. S., El-Aziz, N. K. A., Yousef, S. G., Hefny, A. A., Remele, E. M. A., Shaker, A., & Elsohaby, I. (2023). Molecular characterization and antimicrobial susceptibilities of *Corynebacterium pseudotuberculosis* isolated from caseous lymphadenitis of smallholder sheep and goats. *Animals 13*(14), 2337. https://doi.org/10.3390/ani13142337

Folador, E. L., de Carvalho, P. V. S. D., Silva, W. M., Ferreira, R. S., Silva, A., Gromiha, M., Ghosh, P., Barh, D., Azevedo, V., & Röttger, R. (2016). In silico identification of essential proteins in *Corynebacterium pseudotuberculosis* based on protein-protein interaction networks. *BMC Systems Biology 10*, 103. https://doi.org/10.1186/s12918-016-0346-4

Gomide, A. C. P., Ibraim, I. C., Alves, J. T. C., de Sá, P. G., Silva, Y. R. D. O., Santana, M. P., Silva, W. M., Folador, E. L., Mariano, D. C. B., Castro, T. L. D. P., Barbosa, S., Dorella, F. A., Carvalho, A. F., Pereira, F. L., Leal, C. A. G., Figueiredo, H. C. P., Azevedo, V., Silva, A. & Folador, A. R. C. (2018). Transcript one analysis of *Corynebacterium pseudotuberculosis* biovar e*qui* in two conditions of the environmental stress. *Gene 667*(5), 349-360. https://doi.org/10.1016/j.gene.2018.08.028

Guerrero, J. A. V., Jimenez, R. M. D. O., Dibarrat, J. A., Leon, F.H., Morales-Erasto, V. & Salazar, H. G. M. 2018. Isolation and molecular characterisation of *Corynebacterium pseudotuberculosis* from sheep and goats in Mexico. *Microbial Pathogenesis 117*(1), 304-309. https://doi.org/10.1016/j.micpath.2018.02.031

Hamdan, H. F., Ross, E. E. R., Jalil, M. T. M., Hashim, M. A., & Yahya, M. F. Z. R. 2024. Antibiofilm efficacy and mode of action of Etlingera elatior extracts against Staphylococcus aureus. *Malaysian Applied Biology 53*(1), 27-34. https://doi.org/10.55230/mabjournal.v53i1.2808

Idris, S., & Arifah, A. 2023. Nanoparticles antibiotic delivery system: An alternative treatment protocol for caseous lymphadenitis. *FUDMA Journal of Agriculture and Agricultural Technology 9*(2), 46-57. https://doi.org/10.33003/jaat.2023.0902.06

Herasimenka, Y., Cescutti, P., Noguera, S. C. E., Ruggiero, J. R., Urbani, R., Impallomeni, G., Zanetti, F., Campidelli, S., Prato, M., & Rizzo, R. 2008. Macromolecular properties of cepacian in water and in dimethylsulfoxide. *Carbohydrate Research 343*(1), 228-231. https://doi.org/10.1016/j.carres.2007.10.003

Isa, S. F. M., Hamid, U. M. A., & Yahya, M. F. Z. R. (2022). Treatment with the combined antimicrobials triggers proteomic changes in P. aeruginosa-C. albicans polyspecies biofilms. *ScienceAsia 48*(2), 215-222. http://dx.doi.org/10.2306/scienceasia1513-1874.2022.020

Johari, N. A., Aazmi, M. S., & Yahya, M. F. Z. R. (2023). FTIR spectroscopic study of inhibition of chloroxylenol-based disinfectant against Salmonella enterica serovar Thyphimurium biofilm. *Malaysian Applied Biology 52*(2), 97-107. https://doi.org/10.55230/mabjournal.v52i2.2614

Kamaruzzaman, A. N. A., Mulok, T. E. T. Z., Nor, N. H. M., & Yahya, M. F. Z. R. (2022). FTIR spectral changes in *Candida albicans* biofilm following exposure to antifungals. *Malaysian Applied Biology 51*(4), 57-66. https://doi.org/10.55230/mabjournal.v51i4.11

Krátký, M., Konečná, K., Janďourek, O., Diepoltová, A., Vávrová, P., Voxová, B., ... & Bősze, S. (2023). Insight into the antibacterial action of iodinated imine, an analogue of rafoxanide: a comprehensive study of its anti-staphylococcal activity. *Microbiology Spectrum 11*(3), e03064-22. https://doi.org/10.1128/spectrum.03064-22

Lim, J. Y., May, J. M., & Cegelski, L. (2012). Dimethyl sulfoxide and ethanol elicit increased amyloid biogenesis and amyloid-integrated biofilm formation in *Escherichia coli*. *Applied and Environmental Microbiology 78*(9), 3369-3378. https://doi.org/10.1128/AEM.07743-11

Loncar, K. D., Ferris, R. A., McCue, P. M., Borlee, G. I., Hennet, M. L., & Borlee, B. R. (2017). *In vitro* biofilm disruption and bacterial killing using nonantibiotic compound against Gram-negative equine uterine pathogens. *Journal of Equine Veterinary Science 53*, 94-99. https://doi.org/10.1016/j.jevs.2017.02.003

Maddela, N. R., Zhou, Z., Yu, Z., Zhao, S., & Meng, F. (2018). Functional determinants of extracellular polymeric substances in membrane biofouling: Experimental evidence form pure-cultured sludge bacteria. *Applied and Environmental Microbiology 84*(15), e00756-18. https://doi.org/10.1128/AEM.00756-18

Mihoubi, W., Sahli, E., Gargouri, A., & Amiel, C. (2017). FTIR spectroscopy of whole cells for the monitoring of yeast apoptosis mediated by p53 over-expression and its suppression by *Nigella sativa* extracts. *PLos ONE 12(7*), e0180680. https://doi.org/10.1371/journal.pone.0180680

Nandiyanto, A. B. D., Oktiani, R. & Ragadhita, R. (2019). How to read and interpret FTIR spectroscope of organic material. *Indonesian Journal of Science and Technology 4*(1), 97-118. http://dx.doi.org/10.17509/ijost.v4i1.15806

Nematiasgarabad, P., Hashim, N. A. N., & Yahya, M. F. Z. R. (2024). In silico elucidation of protein-protein interaction network in fish pathogen Flavobacterium Columnare. *Malaysian Applied Biology 53*(3), 137-146. https://doi.org/10.55230/mabjournal.v53i3.2942

Patil, A., Kinoshita, K., & Nakamura, H. (2010). Hub promiscuity in protein-protein interaction networks. *International Journal of Molecular Sciences 11*(4), 1930-1943. https://doi.org/10.3390/ijms11041930

Santi, L., Berger, M., Guimarães, J. A., Calegari-Alves, Y. P., Vainstein, M. H., Yates III, J. R., & Beys-da-Silva, W. O. (2024). Proteomic profile of *Cryptococcus gattii* biofilm: Metabolic shift and the potential activation of electron chain transport. *Journal of Proteomics 290*, 105022. https://doi.org/10.1016/j.jprot.2023.105022

Schwarzer, S., Radzieta, M., Jensen, S. O., & Malone, M. (2021). Efficacy of a topical wound agent methanesulfonic acid and dimethysulfoxide on in vitro biofilms. *International Journal of Molecular Science 22*, 9471. https://doi.org/10.3390/ijms22179471

Summer, K., Browne, J., Hollanders, M., & Benkendorff, K. (2022). Out of control: The need for standardized solvent approaches and data reporting in antibiofilm assays incorporating dimethyl-sulfoxide (DMSO). *Biofilm 4*(2), 100081. https://doi.org/10.1016/j.bioflm.2022.100081

Tavares, I. F., de Sá, M. D. C. A., Rocha Filho, J. T. R., Trindade, S. C., Fraga, R. E., & Meyer, R. (2024). Immune response of BALB/c mice infected with two strains of Corynebacterium pseudotuberculosis. *Microbial Pathogenesis*

192, 106671. https://doi.org/10.1016/j.micpath.2024.106671

Xu, S., Ping, Z., Xu, X., & Zhang, L. (2016). Changes in shape and size of the stiff branched β-glucan in dimethlysulfoxide/water solutions. *Carbohydrate polymers 138*, 86-93. https://doi.org/10.1016/j.carbpol.2015.11.049

Yaacob, M. F., Murata, A., Nor, N. H. M., Jesse, F. F. A., & Yahya, M. F. Z. R. Y. 2021. Biochemical composition, morphology and antimicrobial susceptibility pattern of *Corynebacterium pseudotuberculosis* biofilm. *Journal of King Saud University Science 33*(1), 101225. https://doi.org/10.1016/j.jksus.2020.10.022

Yahya, M. F. Z. R. Y., Alias, Z., & Karsani, S. A. (2017). Subtractive protein profiling of *Salmonella typhimurium* biofilm treated with DMSO. *The Protein Journal 36*, 286-298. https://doi.org/10.1007/s10930-017-9719-9

Yahya, M. F. Z. R. Y., Alias, Z., & Karsani, S. A. (2018). Antibiofilm activity and mode of action of DMSO alone and its combination with afatinib against Gram-negative pathogens. *Folia Microbiologica 63*(1), 23-30. https://doi.org/10.1007/s12223-017-0532-9

Yahya, M. F. Z. R., Nor, N. H. M., Mahat, M. M., & Siburian, R. 2024. Edible coating, food-contact surface coating, and nanosensor for biofilm mitigation plans in food industry. *Food Materials Research 4*(1), e025. https://doi.org/10.48130/fmr-0024-0016

Yakup, N. F., Nor, N. H. M., Mahat, M. M., Siburian, R., & Yahya, M. F. Z. R. (2024). Unveiling the Antibiofilm Arsenal: A Mini Review on Nanoparticles' Mechanisms and Efficacy in Biofilm Inhibition. In *International Conference on Science Technology and Social Sciences–Physics, Material and Industrial Technology (ICONSTAS-PMIT 2023)*. pp. 177-185. Atlantis Press. https://doi.org/10.2991/978-94-6463-500-3_16

Zawawi, W. M. A. W. M., Ibrahim, M. S. A., Rahmad, N., Hamid, U. M. A., & Yahya, M. F. Z R. (2020). Proteomic analysis of Pseudomonas aeruginosa biofilm treated with Chromolaena odorata extracts. *Malaysian Journal of Microbiology 16*(2), 124-133. http://dx.doi.org/10.21161/mjm.190512

Zulkiply, N., Yunus, N. M., Idris, H., Noor, W. S. A., W. M., Karsani, S. A., Yahya, M. F. Z. R. (2024). In silico and MS/MS-based approaches to investigate protein-protein interaction networks in Staphylococcus aureus biofilm. *Malaysian Journal of Analytical Science 28*(4), 939-955.

Zuurmond, W. W., Langendijk, P. N., Bezemer, P. D., Brink, H. E., de Lange, J. J., Van Loenen, A. C. (1996) Treatment of acute reflex sympathetic dystrophy with DMSO 50% in a fatty cream. *Acta Anaesthesiologica Scandinavica 40*(3), 364–367. https://doi.org/10.1111/j.1399-6576.1996.tb04446.x